

High-Performance Biodegradable/Transient Electronics on Biodegradable Polymers

Suk-Won Hwang, Jun-Kyul Song, Xian Huang, Huanyu Cheng, Seung-Kyun Kang, Bong Hoon Kim, Jae-Hwan Kim, Sooyoun Yu, Yonggang Huang, and John A. Rogers*

Biodegradable polymers are used extensively in medical devices. Examples include carriers for controlled drug release and scaffolds for tissue engineering.^[1–7] The ability to integrate fully biodegradable, high-performance electronics and sensors with these materials could significantly expand the functional capabilities in medicine, with additional implication in areas such as consumer electronics and environmental sensors, where degradability could eliminate waste streams associated with recycling/disposal and practical difficulties in device collection/recovery, respectively. Work toward this goal involves strategies that range from use of ultra-miniaturized device components^[8,9] to organic/bio-organic active materials.^[10–12] More recent approaches exploit high performance (i.e., intrinsic properties such as mobilities and on/off ratios of transistors that approach values comparable to those found in commercial electronics) biodegradable semiconductors, such as ultrathin films of silicon and metal oxides, with appropriate metals and inorganic dielectrics.^[13–16] Advanced schemes allow integration of fully formed device elements of this type with degradable substrates.^[15] Here, a final set of processing steps defines electrical interconnects and other features to yield completed systems. Published examples include RF harvesters, solar modules, ring

oscillators and logic gates. A key challenge is that the substrate materials must have the necessary chemical resistance and temperature stability to accommodate this processing. Examples in the literature avoid these issues by, for instance, use of shadow masks, rather than photolithography and etching, to define the interconnect structures. Severe limitations in resolution and materials options associated with this approach. For example, use of shadow masks does not allow feature sizes below several microns, and processing must be performed well below the glass transition temperature of the substrate material. This situation motivates the development of alternative strategies. In the following, we introduce a fabrication approach whose key feature is that it separates processing of the electronic systems from the target device substrate. Here, transfer of the complete structure, including interconnects, from a temporary substrate where it is fabricated to a final device substrate for its operation avoids constraints associated with the intrinsic properties of biodegradable polymers and thereby enables mounting on nearly any surface or class of material. We demonstrate these schemes in various representative devices and arrays, with a range of degradable substrate materials, including poly lactic-co-glycolic acid (PLGA), a copolymer of poly lactic acid (PLA) and poly glycolic acid (PGA), PLA, polycaprolactone (PCL) and rice paper. The resulting systems can be laminated onto various other supporting surfaces with either planar or non-planar shapes. The content begins with descriptions of these procedures and mechanical/chemical considerations in materials selection. Various demonstrations, including devices that incorporate functional arrays of hydration sensors, illustrate the capabilities.

The key to expanding the materials options is to separate deposition, etching and lithographic patterning associated with fabrication of the electronic components from the biodegradable substrates. **Figure 1a** describes procedures that begin with spin casting of a sacrificial layer of poly (methylmethacrylate) (PMMA, MicroChem, USA) followed by an ultrathin layer of diluted polyimide (D-PI) (~200 nm) on a silicon (Si) wafer. Transfer printing then delivers patterned, doped silicon nanomembranes (Si NMs) or fully formed ultrathin silicon microdevices to the surface of the D-PI layer in spatial layouts that match requirements. Depositing other materials and patterning them by photolithography yield completed systems of electronics, integrated sensors and/or power supplies. For examples reported here, these steps include plasma-enhanced chemical vapor deposition (PECVD) of SiO₂ (~50 nm) for gate and interlayer dielectrics, and Mg (~300 nm) for source, drain, gate contacts, and interconnects. Afterward, spin casting

Dr. S.-W. Hwang, J.-K. Song, Dr. X. Huang,
Dr. S.-K. Kang, Dr. B. H. Kim, J.-H. Kim
Department of Materials Science and Engineering
and Frederick Seitz Materials Research Laboratory
University of Illinois at Urbana-Champaign, Urbana
IL 61801, USA



H. Cheng, Prof. Y. Huang
Department of Mechanical Engineering
Civil and Environmental Engineering
Center for Engineering and Health
and Skin Disease Research Center
Northwestern University, Evanston
IL 60208, USA

S. Yu
Department of Chemical and Biomolecular Engineering
University of Illinois at Urbana-Champaign, Urbana
IL 61801, USA

Prof. J. A. Rogers
Department of Materials Science and Engineering
Chemistry, Mechanical Science and Engineering
Electrical and Computer Engineering
Beckman Institute for Advanced Science and Technology
and Frederick Seitz Materials Research Laboratory
University of Illinois at Urbana-Champaign, Urbana
IL 61801, USA
E-mail: jrogers@illinois.edu

DOI: 10.1002/adma.201306050

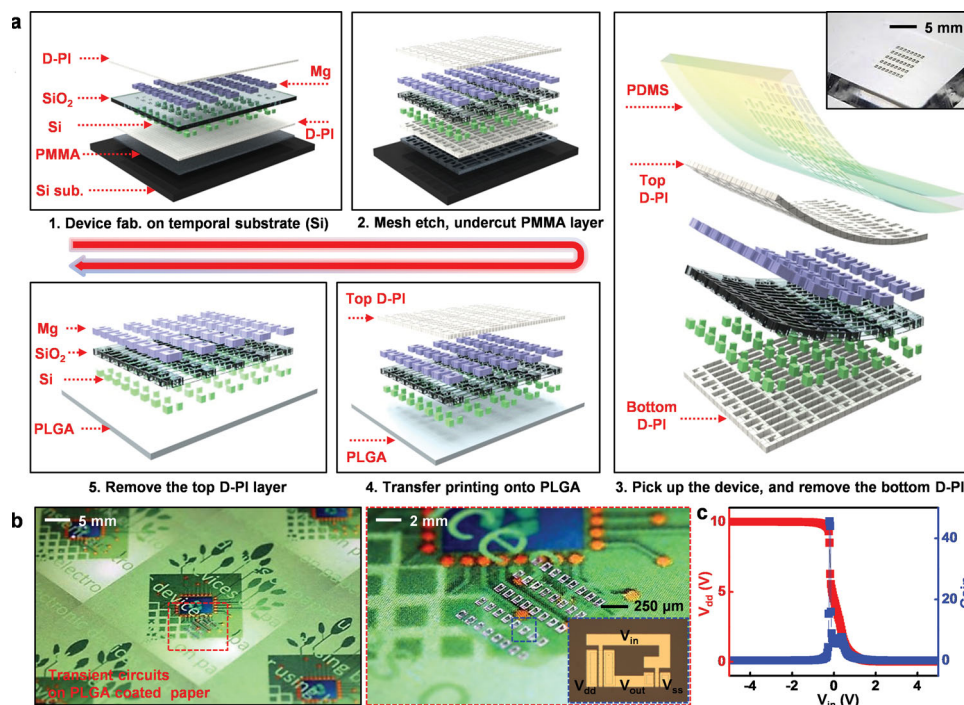


Figure 1. Materials and procedures for fabricating transient electronic circuits on biodegradable substrates. (a) Schematic illustrations of key processes for fabricating transient complementary metal-oxide-semiconductor (CMOS) on a carrier substrate (upper left). Defining a mesh type structure allows dissolution of the PMMA layer in boiling acetone at 90 °C to release the entire device (upper middle). Retrieving the released device onto a PDMS stamp (right, image of the device on PDMS in the inset), allows exposure and removal of the bottom layer of D-PI by reactive ion etching. Transfer printing onto a PLGA substrate (lower middle), and RIE etching of the top D-PI completes the process (lower left). (b) Images showing an array of transient CMOS inverters on a piece of paper coated with PLGA (left), with magnified view (right), and microscope image of an inverter in the inset. (c) Output voltage characteristics of a representative CMOS inverter with $V_{dd} = 10$ V. The voltage gain is ~ 50 .

defines another layer of D-PI, uniformly on top of the resulting set of devices. Etching openings in certain regions of the polymers (D-PI, PMMA) and, if necessary, other layers such as the SiO_2 , exposes the PMMA at the base. Immersing a sample processed in this way in acetone removes the PMMA, to release an ultrathin circuit that can be lifted from the Si wafer onto the surface of a slab of PDMS using the techniques of transfer printing. Next, reactive ion etching (O_2 gas, March RIE) eliminates the exposed, bottom layer of D-PI while the structure is still on the PDMS. Transfer to a biodegradable substrate allows removal of the top layer of D-PI, using reactive ion etching again, to complete the process. The image in the left frame of Figure 1b presents an array of transient Si n- and p-channel transistors on a coating of PLGA cast on a sheet of paper with printed text and logos. A magnified view appears in the right frame of Figure 1b, with a microscope image of a representative device in the inset. Figure 1c provides measurement results from a complementary metal-oxide-semiconductor (CMOS) inverter. The gain and threshold voltage (V_{th}) are ~ 50 and -1 V with $V_{dd} = 10$ V, respectively. The performance is comparable to that of devices prior to transfer, and of results achieved using low resolution shadow masking techniques reported previously.^[14]

The versatility of these schemes and their compatibility with nearly any class of substrate motivate consideration of desired properties in the materials. The choice of biodegradable polymers was guided partly by the ability to induce some level of

tackiness on their surfaces, for purpose of increased yield in transfer. PLGA is one of the most popular such materials because its properties can be tuned by adjusting molecular weight and the ratio of lactide to glycolide. In water, PLGA undergoes degradation via hydrolysis of its ester linkages. Increasing the lactide content increases the hydrophobicity and decreases the water absorption, thereby reducing the degradation rate. PCL, as one of earliest studied biopolymers, is also of interest, partly because of its wide commercial availability. This polymer is hydrophobic and semi-crystalline, with a degree of crystallinity that can be tuned by molecular weight and processing conditions. The advantages of PCL include adjustable degradation kinetics and availability of simple procedures for casting and shaping.^[6] Rice paper provides another option, due to its low cost availability, and suitability in ingestible device embodiments.

Flexible transient electronic systems can be formed on films of these or other biopolymers, with subsequent possibility for integration onto various other supports, ranging from sheets of paper to gloves. Thin layers of PLGA can serve as adhesives in these cases. Figure 2a presents a photograph of an array of transient CMOS inverters on a thin film of PLGA (15 ~ 20 μm thick), wrapped on a glass rod, including a magnified image in the inset. In addition to spin-casting, use of melt processing, electrospinning^[17] and other methods can provide additional options in preparing the polymer substrates. Figure 2b and 2c show images of a transient Si CMOS inverter circuit on PCL

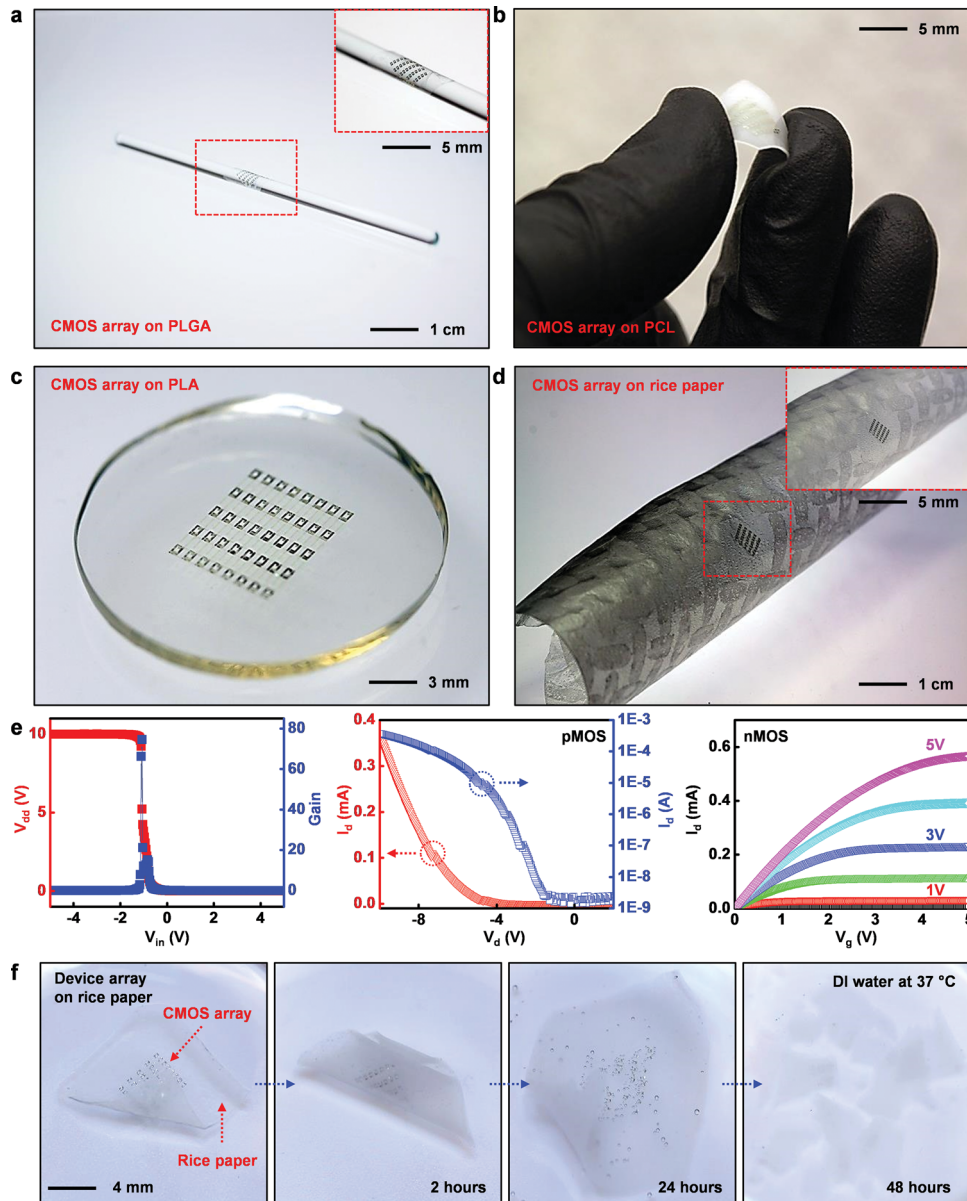


Figure 2. Transient electronic systems on biodegradable polymers and rice paper. (a) Photograph of an array of transient CMOS inverters on a thin PLGA substrate wrapped onto a cylindrical glass rod, with a magnified image in the inset. (b) Image of a transient device on a PCL substrate, in a bent configuration. (c) An array of transient CMOS inverters on a PLA substrate. (d) Image of a transient circuit on rice paper. Here, a small amount of water creates a slightly tacky surface to facilitate transfer. (e) Output voltage characteristics of a representative CMOS inverter at $V_{dd} = 10$ V. The gain is ~ 80 (left). Linear (red) and log scale (blue) transfer curves of a typical transient p-channel MOSFET (middle). The channel length (L) and width (W) are $5 \mu\text{m}$ and $300 \mu\text{m}$, respectively. The mobility (linear regime) and on/off ratio are $\sim 70 \text{ cm}^2/\text{V}\cdot\text{s}$ and $\sim 10^5$, respectively. I-V characteristics of a typical n-channel MOSFET (right). The channel length (L) and width (W) are $15 \mu\text{m}$ and $100 \mu\text{m}$, respectively. The mobility (linear regime) and on/off ratio are $\sim 400 \text{ cm}^2/\text{V}\cdot\text{s}$ and $\sim 10^5$, respectively. (f) Optical images at various stages of dissolution of an array of transient CMOS inverter on rice paper during immersion in DI water at physiological temperature (37°C).

(~ 1 mm thick) and PLA (~ 1 mm thick), respectively. Both polymers provide sufficient tackiness to ensure release during transfer printing at elevated temperatures ($150 \sim 180^\circ\text{C}$). Figure 2d illustrates a similar transient CMOS system on rice paper ($\sim 200 \mu\text{m}$ thick). Here, applying a small amount of water to the surface of the substrate softens the material in a way that facilitates transfer. Additional images appear in Figure S1. Figure 2e shows the measured electrical characteristics of a typical

CMOS inverter (left) and individual p- (middle) and n-channel (right) metal-oxide-semiconductor field-effect transistors (MOSFETs). The gain and threshold voltage (V_{th}) are ~ 80 and -1 V, respectively. The negative threshold voltage of the inverters likely arises from the high negative threshold voltage (~ -5 V) of the p-type MOSFETs. The mobilities, calculated from the saturation and linear regime, are $\sim 60 \text{ cm}^2/\text{V}\cdot\text{s}$ and $\sim 70 \text{ cm}^2/\text{V}\cdot\text{s}$ for the p-channel devices, and $\sim 350 \text{ cm}^2/\text{V}\cdot\text{s}$ and $\sim 400 \text{ cm}^2/\text{V}\cdot\text{s}$ for the

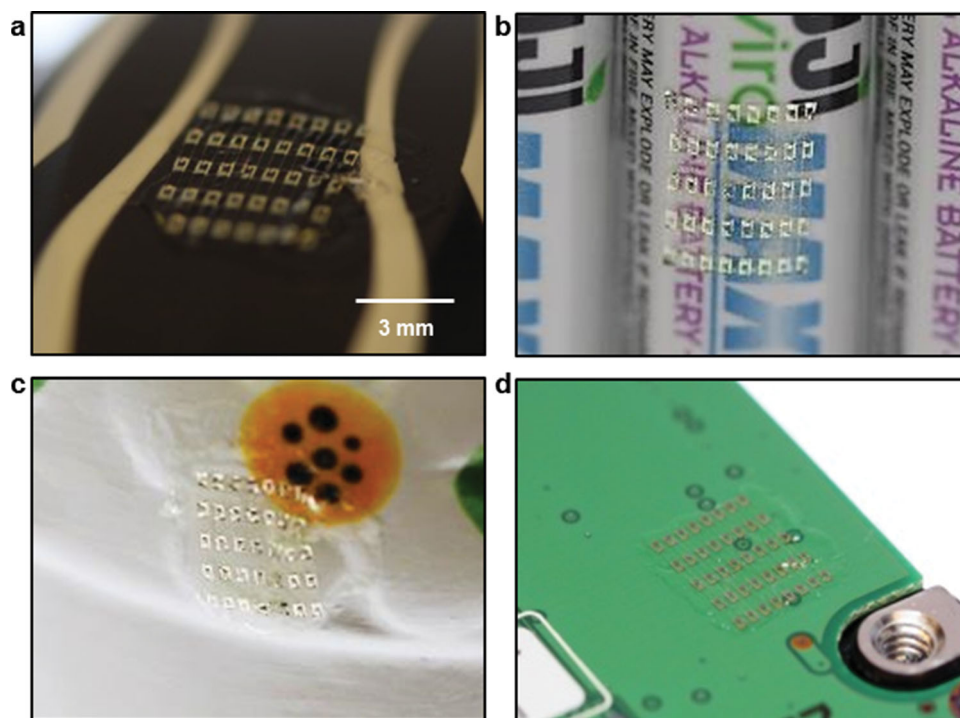


Figure 3. Illustration of transient/biodegradable electronic circuits in configurations relevant to envisioned applications. (a) Surveillance system (drone). (b) Green electronics (batteries). (c) Eco-friendly merchandise (plants). (d) Degradable electronic devices that minimize waste streams (portable devices).

n-channel devices, respectively. The on/off current ratios (I_{on}/I_{off}) are $\sim 10^5$ for both types of transistors. When stored in a dry environment, the devices showed stable operation.

Figure 2f provides a set of images collected during dissolution of a system on rice paper (Figure 2d), at various times after immersion in deionized (DI) water at 37 °C. Here, rice paper rapidly absorbs water and begins to swell, thereby leading to disintegration of the array into individual devices. Each component then gradually disappears in a manner defined by the dissolution rates of various constituent materials.^[13] Hydrolysis consumes the Mg electrodes in several hours. Dissolution of PECVD SiO₂ and Si in phosphate buffer solutions (PBS, pH 7.4) at physiological temperature occurs on a timescale of weeks. In all cases, the rates for complete disappearance depend strongly on temperature, pH, ionic content, thickness and morphology.

Potential applications of transient/ biodegradable electronics range from anti-tamper systems, green/eco-friendly electronics to implantable devices. **Figure 3** shows representative substrates that have generic relevance to these and other classes of applications: security systems (Figure 3a), environmental sensors (Figure 3b and 3c) and green/compostable electronics (Figure 3d).

To illustrate a technological example in medicine, consider a transient hydration sensor that might be used as an applique to monitor healing processes at the site of a wound on the skin, constructed on a PLGA substrate. Hydration levels play critical roles in wound healing. Excessive hydration can cause maceration of the wound, while dehydration can delay wound recovery.^[18–21] **Figure 4a** shows an image of a device, with a magnified view in the inset (left), and exploded-view schematic

illustration (right). This system consists of eight separate channels with four measuring electrodes and four reference electrodes. The electrode geometries include circular and interdigitated designs. The device uses phosphorous doped silicon ($\sim 10^{20}$ cm⁻³) for the electrodes (~ 300 nm), magnesium (Mg) for contacts/interconnects (200 ~ 250 nm), PECVD silicon dioxide (SiO₂) for the interlayer dielectrics (~ 100 nm) and PLGA for the substrate (~ 20 μ m). A demonstration of operation involves applying lotion to the skin and then measuring frequency-dependent changes in the impedance as a function of time. The amplitude of the impedance measured at each channel changes monotonically with the level of skin hydration. After subtracting impedances associated with the measuring electrodes from the reference electrodes, the frequency-response of the device at different hydration levels can be obtained from circular (left) and interdigitated (right) electrode formats, as shown in Figure 4b. As the hydration levels changes from 119 to 16.7 (arbitrary units, determined by a commercial hydration meter (CMM)), the differential impedance amplitude at 15 kHz decreases steadily from ~ 0.79 M Ω and ~ 1.2 M Ω for circular and interdigitated electrodes, respectively. At a fixed hydration level of 16.7, the differential impedance amplitude decreases from 0.866 M Ω at 15 kHz to 25 k Ω at 95 kHz for circular electrodes. These behaviors are similar to those observed previously in conformal, non-transient ‘epidermal’ sensors.^[22] The changes are related to variations in the conductivity and permittivity of the skin, due likely to changes in the water and ionic content of the skin.^[23–26] Experimental results in Figure 4b can be converted into hydration levels using reference values from the CMM through least square fitting (Figure 4c). The converted data

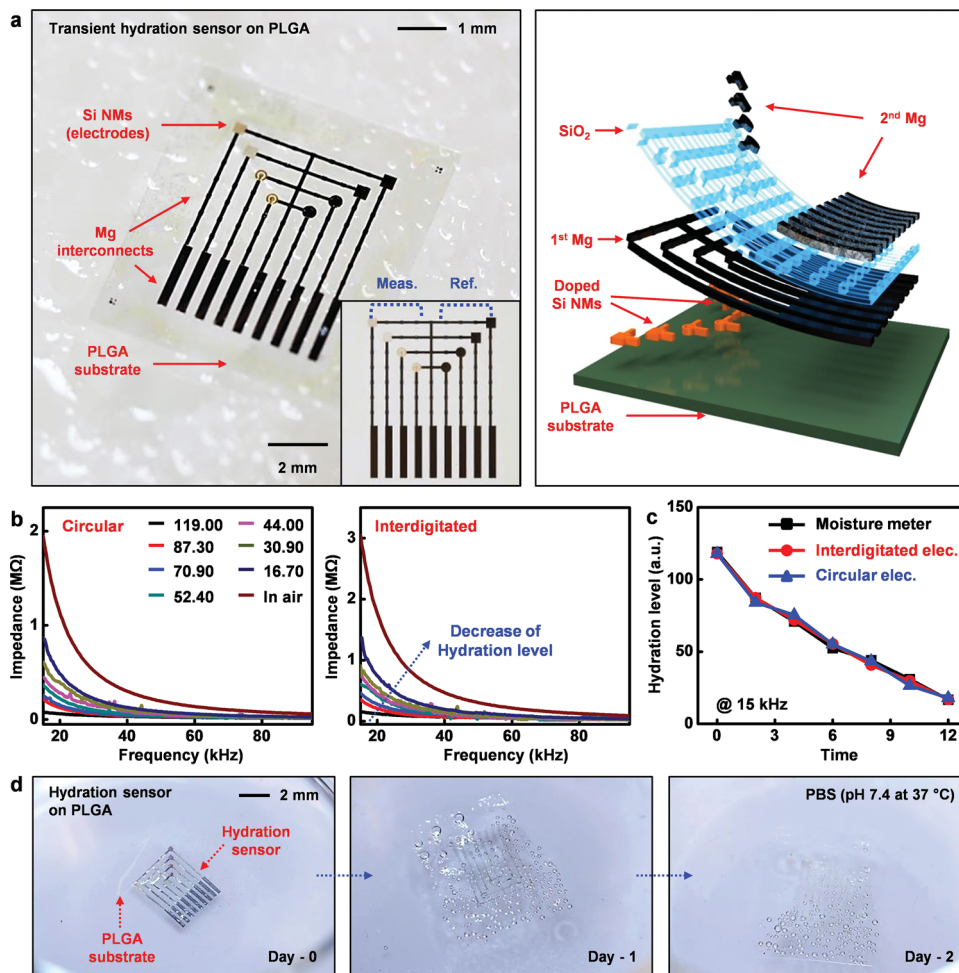


Figure 4. A transient hydration sensor. (a) Image and exploded-view schematic illustration of a transient hydration sensor, comprised of doped Si NMs for electrodes, Mg for contacts and interconnects, PECVD SiO₂ as interlayer dielectrics and PLGA for the substrate. (b) Results from use of this type of device to measure changes in impedance as a function of frequency, with both circular (left) and interdigitated (right) electrodes. (c) Comparison of hydration levels measured using a commercial moisture meter (CMM, MoistureMeterSC Compact, Delfin Inc) and a transient hydration sensor (black, moisture meter; red, circular electrodes; blue, interdigitated electrodes). (d) Images of a transient hydration sensor on a PLGA film at various stages of dissolution during immersion in phosphate buffer solutions (PBS, 1M, pH 7.4) at physiological temperature (37 °C) after 1 day and 2 days, respectively.

are consistent with the CMM and with the transient hydration sensor in both electrode formats. Over a measurement period of approximately 12 minutes, deviations between the hydration levels from the CMM and calibrated values from the transient sensor are less than 14% and 7%, respectively. In vitro test for the effect of a protein layer on this type of measurements appears in Figure S2. Previously described approaches^[13,15] for sterilizing the devices can be used for the system reported here.

Figure 4d provides dissolution behaviors of a transient hydration sensor on PLGA substrate, at various times while submerged in phosphate buffer solution (PBS, 1M, pH 7.4, Sigma-Aldrich, USA) at physiological temperature (37 °C). Upon immersion, the exposed magnesium (2nd Mg) disappears quickly, while the underlying Mg (1st Mg) slowly dissolves due to its encapsulation with PECVD SiO₂. Here, Si and PECVD SiO₂ will completely dissolve in days or weeks,^[13] the PLGA will dissolve over some months.^[1,3]

During dissolution, substrate materials such as PLGA can swell; this swelling can lead to fracture/disintegration of the

supported device structures. These phenomena are important because they can disrupt device behavior prior to dissolution of the constituent materials. Mechanics analysis provides insights. Consider, for example, various thin film structures relevant to transient electronics (Figure 4a): PLGA/Si/Mg/SiO₂/Mg, PLGA/Si/Mg/SiO₂, PLGA/Mg/SiO₂/Mg, PLGA/Mg/SiO₂. As a point of reference, consider also bare PLGA. Due to the high stiffness of the device layers, the system bends upward upon a swelling strain of $\epsilon_{\text{swelling}}$ in the PLGA. The bending curvature κ is related to the bending stiffness \overline{EI}_i of each layered structure as

$$\kappa = \frac{E'_{\text{sub}} \epsilon_{\text{swelling}}}{\sum_{i=1}^5 \alpha_i \overline{EI}_i} \left(\sum_{i=1}^5 \alpha_i b_i - \frac{h_{\text{sub}}}{2} \right) h_{\text{sub}}, \quad (1)$$

where E'_{sub} and h_{sub} are the biaxial modulus and thickness of the PLGA substrate, α_i is the area percentage of each layered structure out of the total area and b_i is the distance from the

neutral mechanical plane (NMP) of each layered structure to the bottom surface of the PLGA. The bending induces a compressive strain above the NMP, thereby reducing the tensile strain $\varepsilon_{\text{swelling}}$ from swelling to yield a strain, given by

$$\varepsilon_i = \frac{E'_{\text{sub}} h_{\text{sub}}}{EA_i} \varepsilon_{\text{swelling}} - \kappa(z - b_i), \quad (2)$$

where z is the distance measured from the bottom surface of the PLGA substrate, and \overline{EI}_i is the tensile stiffness of each layered structure. For a swelling of 18% in the PLGA, the maximum strain calculated from Equation (2) is 4.90 % in Si and 7.61% in SiO₂, which exceed the fracture strains of Si and SiO₂ (~1%). Fracture would therefore be expected to occur in this system. Calculations suggest that, to avoid fracture, relatively thick active layers (Si of 500 nm /Mg of 500 nm /SiO₂ of 400 nm /Mg of 100 nm) and thin substrates (10 μm), with swelling less than 7%, are required. Alternatively, the concepts of stretchable electronics could be exploited through appropriate structuring of the materials to allow in and out of plane mechanical buckling of the active materials in response to swelling of the substrate. The relevant functional time period of the system could be simply defined by swelling and associated fracture, rather than dissolution. Swelling of PLGA, for example, occurs slowly during the first few days of immersion in aqueous solution, and this rate can be adjusted by molecular weights and/or ratios of PLA to PGA.^[27,28]

The concepts introduced here provide materials, manufacturing strategies and device designs for transient electronic circuits that can be integrated onto biodegradable polymer substrates. The combined use of transient devices, comprised of inorganic materials with biopolymer substrates, provides versatility in engineering desired behaviors. Additional considerations in mechanics and fracture can be important in determining the operating lifetimes and optimized system geometries.

Experimental Section

Fabrication of Transient Silicon Complementary Metal-Oxide-Semiconductor (CMOS) Inverters: Three different doping procedures were performed on n-type silicon on insulator (SOI, top silicon ~260 nm, SOITEC, France) wafers. Boron doping at 550 °C using spin-on dopant (SOD, Filmtronics, USA) defined lightly doped regions for the p-wells (p⁻). Heavily doped p-type regions for source and drain electrodes were formed at 1050 °C for p-type transistors. Phosphorous doping at 950 °C defined highly doped areas for source and drain contacts for n-type transistors. Removal of the buried oxide by wet etching with HF released the top device silicon from the SOI, and enabled their transfer printing onto a spin cast film of PMMA/D-PI on silicon carrier substrate. Doped silicon nanomembranes (Si NMs) were isolated by reactive ion etching (RIE; Plasmatherm) with sulfur hexafluoride (SF₆) gas. A thin layer of SiO₂ (~50 nm) formed by plasma-enhanced chemical vapor deposition (PE-CVD) served as the gate dielectric. Etching openings in this layer using a buffered oxide etchant (BOE, Transene Company Inc., USA) defined contact pads for source and drain electrodes. A 300 nm layer of Mg (deposited by electron beam evaporation) was used for source, drain, gate electrodes, as well as interconnects. Another thin layer of D-PI was cast on top of the Mg. Patterned etching removed certain regions of the polymer layers (D-PI, PMMA) and SiO₂, to create an open mesh structure that facilitated dissolution of the underlying sacrificial

layer of PMMA. This process involved immersion in acetone to release an ultrathin circuit from the carrier substrate, suitable for retrieval onto the surface of a slab of PDMS. The bottom layer of D-PI was removed by reactive ion etching (RIE) using oxygen (O₂) gas, and the circuit was transfer printed onto a biodegradable polymer. Finally, the top layer of D-PI was removed by RIE.

Fabrication Method for a Transient Hydration Sensor: To form eight separate electrodes, doped monocrystalline silicon nanomembranes (thickness ~300 nm, p-type) were constructed on SOI wafers, using phosphorous spin-on dopant at 950 °C. Approaches similar to those described in the previous section were used for device fabrication. The measuring and reference electrodes were defined by RIE. Layers of Mg and SiO₂ served as contacts/interconnects and interlayer dielectrics, respectively.

Electrical Characterizations of a Transient Hydration Sensor: A data acquisition system (DAQ) equipped with an impedance analyzer chip (AD5933, Analog Devices) and a multiplexer (ADG 708, Analog Devices) for switching between electrodes allowed measurements using the hydration sensor. Details appear elsewhere.^[22] Briefly, an alternating current (AC) voltage (2V, peak to peak) at frequencies between 15 kHz and 95 kHz was generated from the impedance analyzer and introduced to each of the electrodes of the hydration sensor through the multiplexer. The amplitude and phase of the reflected voltage from the skin was received by the common ground of the hydration sensor, and converted to impedance levels within the impedance analyzer. The hydration sensor was connected to the DAQ with anisotropic conductive film (ACF) cables. During in-vivo experiments, the sensor was attached to the skin of ventral forearm to reveal frequency dependent changes in impedance associated with application of moisturizing lotions (Intensive Rescue Moisture Body Lotion, Vaseline Inc.). A commercial moisture meter (CMM) (MoistureMeter SC Compact, Delfin Inc)^[22] served as a reference to enable conversion of impedance values to hydration levels.

Supporting Information

Supporting Information is available from the Wiley Online Library or from the author.

Acknowledgements

Huanyu Cheng is a Howard Hughes Medical Institute International Student Research fellow. The facilities for characterization and analysis were provided by the Material Research Laboratory and Center for Microanalysis of Materials at the University of Illinois at Urbana-Champaign, both of which are supported by the U.S. Department of Energy. The research was funded by an NSF INSPIRE grant.

Received: December 10, 2013

Revised: February 12, 2014

Published online: April 1, 2014

- [1] X. S. Wu, N. Wang, *J. Biomater. Sci. Polymer Edn.* **2001**, *12*, 21.
- [2] T. Ponnusamy, L. B. Lawson, L. C. Freytag, D. A. Blake, R. S. Ayyala, V. T. John, *Biomater* **2012**, *2*, 77.
- [3] H. K. Makadia, S. J. Siegel, *Polymers* **2011**, *3*, 1377.
- [4] M. I. Sabir, X. Xu, L. Li, *J. Mater. Sci.* **2009**, *44*, 5713.
- [5] C. X. F. Lam, M. M. Savalani, S.-H. Teoh, D. W. Huttmacher, *Biomed. Mater.* **2008**, *3*, 034108.
- [6] M. A. Woodruff, D. W. Huttmacher, *Prog. Polym. Sci.* **2010**, *35*, 1217.
- [7] D. W. Huttmacher, *J. Biomater. Sci. Polymer Edn.* **2001**, *12*, 107.
- [8] D.-H. Kim, Y.-S. Kim, J. Amsden, B. Panilaitis, D. L. Kaplan, F. G. Omenetto, M. R. Zakin, J. A. Rogers, *Appl. Phys. Lett.* **2009**, *95*, 133701.

- [9] D. -H. Kim, J. Viventi, J. Amsden, J. Xiao, L. Vigeland, Y.-S. Kim, J. A. Blanco, B. Panilaitis, E. S. Frechette, D. Contreras, D. L. Kaplan, F. G. Omenetto, Y. Huang, K.-C. Hwang, M. R. Zakin, B. Litt, J. A. Rogers, *Nat. Mater.* **2010**, *9*, 511.
- [10] C. J. Bettinger, Z. Bao, *Adv. Mater.* **2010**, *22*, 651.
- [11] M. Irimia-Vladu, P. A. Troshin, M. Reisinger, L. Shmygleva, Y. Kanbur, G. Schwabegger, M. Bodea, R. Schwödiauer, A. Mumyatov, J. W. Fergus, V. F. Razumov, H. Sitter, N. S. Sariciftci, S. Bauer, *Adv. Funct. Mater.* **2010**, *20*, 4069.
- [12] C. Legnani, C. Vilani, V. L. Calil, H. S. Barud, W. G. Quirino, C. A. Achete, S. J. L. Ribeiro, M. Cremona, *Thin Solid Films* **2008**, *517*, 1016.
- [13] S.-W. Hwang, H. Tao, D.-H. Kim, H. Cheng, J.-K. Song, E. Rill, M. A. Brenckle, B. Panilaitis, S. M. Won, Y. S. Kim, Y. M. Song, K. J. Yu, A. Ameen, R. Li, Y. Su, M. Yang, D. L. Kaplan, M. R. Zakin, M. J. Slepian, Y. Huang, F. G. Omenetto, J. A. Rogers, *Science* **2012**, *337*, 1640.
- [14] S.-W. Hwang, X. Huang, J.-H. Seo, J.-K. Song, S. Kim, S. Hage-Ali, H.-J. Chung, H. Tao, F. G. Omenetto, Z. Ma, J. A. Rogers, *Adv. Mater.* **2013**, *25*, 3526.
- [15] S.-W. Hwang, D.-H. Kim, H. Tao, T.-I. Kim, S. Kim, K. J. Yu, B. Panilaitis, J.-W. Jeong, J.-K. Song, F. G. Omenetto, J. A. Rogers, *Adv. Funct. Mater.* **2013**, *23*, 4087.
- [16] C. Dagdeviren, S.-W. Hwang, Y. Su, S. Kim, H. Cheng, O. Gur, R. Haney, F. G. Omenetto, Y. Huang, J. A. Rogers, *Small* **2013**, *9*, 3398.
- [17] T. D. Brown, P. D. Dalton, D. W. Huttmacher, *Adv. Mater.* **2011**, *23*, 5651.
- [18] M. Hara-Chikuma, A. S. Verkman, *J. Mol. Med.* **2008**, *86*, 221.
- [19] M. Gray, D. Weir, *J. Wound. Ostomy. Cont.* **2007**, *34*, 153.
- [20] T. Minematsu, Y. Yamamoto, T. Nagase, A. Naito, K. Takehara, S. Iizaka, K. Komagata, L. Huang, G. Nakagami, T. Akase, M. Oe, K. Yoshimura, T. Ishizuka, J. Sugama, H. Sanada, *J. Dermatol. Sci.* **2011**, *62*, 160.
- [21] D. R. Thomas, T. R. Cote, L. Lawhorne, S. A. Levenson, L. Z. Rubenstein, D. A. Smith, R. G. Stefanacci, E. G. Tangalos, J. E. Morley, *J. Am. Med. Dir. Assoc.* **2008**, *9*, 292.
- [22] X. Huang, W.-H. Yeo, Y. Liu, J. A. Rogers, *Biointerphases* **2012**, *7*, 52.
- [23] C. Gabriel, S. Gabriel, E. Corthout, *Phys. Med. Biol.* **2006**, *41*, 2231.
- [24] C. Gabriel, A. Peyman, E. H. Grant, *Phys. Med. Biol.* **2009**, *54*, 4863.
- [25] T. Sunaga, H. Ikehira, S. Furukawa, H. Shinkai, H. Kobayashi, Y. Matsumoto, E. Yoshitome, T. Obata, S. Tanada, H. Murata, Y. Sasaki, *Phys. Med. Biol.* **2002**, *47*, N11.
- [26] V. Raicu, N. Kitagawa, A. Irimajiri, *Phys. Med. Biol.* **2000**, *45*, L1.
- [27] L. K. Chiu, W. J. Chiu, Y.-L. Cheng, *Int. J. Pharm.* **1995**, *126*, 169.
- [28] L. Solorio, A. M. Olear, J. I. Hamilton, R. B. Patel, A. C. Beiswenger, J. E. Wallace, H. Zhou, A. A. Exner, *Theranostics* **2012**, *2*, 1064.